

Reinterpretation of ATLAS and CMS searches in monojet and mono- V final states: prospects of limits on excited neutrinos

Gabriela Karkosova Martinovicova,^a Vojtech Pleskot^a

^a*Faculty of Mathematics and Physics, Charles University, Prague, Czech Republic*

E-mail: gabriela.martinovicova@matfyz.cuni.cz,
vojtech.pleskot@matfyz.cuni.cz

ABSTRACT: Searches for final states with large missing transverse momentum recoiling against a jet or a hadronically decaying vector boson provide strong constraints on a wide class of physics scenarios beyond the Standard Model. In this work, we reinterpret existing ATLAS and CMS monojet and mono- V searches at $\sqrt{s} = 13$ TeV in the context of excited-neutrino production. Published signal-region selections, post-fit background estimates, and observed event yields are used with simulated excited-neutrino signals to derive upper limits on the production cross-section as a function of the excited-neutrino mass. The monojet searches allow excited-neutrino masses of up to approximately 4 TeV to be excluded for representative benchmark scenarios. Mono- V searches provide constraints on the parameter space region with large couplings to the SM electroweak gauge bosons and low excited-neutrino masses compared to the compositeness scale. This is complementary to the region probed by the monojet searches.

KEYWORDS: Hadron Colliders, Beyond Standard Model, Fermion Compositeness, Excited Neutrino

Contents

1	Introduction	1
2	Theoretical Framework	2
3	Signal Generation and Detector Simulation	3
4	Reinterpretation of the ATLAS monojet search	5
5	Reinterpretation of the CMS monojet and mono-V search	6
6	Conclusion	10

1 Introduction

The search for physics beyond the Standard Model (SM) is one of the key objectives of the Large Hadron Collider (LHC). Final states featuring large missing transverse momentum, $\mathbf{p}_T^{\text{miss}}$, recoiling against a single energetic jet or vector boson, commonly referred to as monojet or mono- V signatures, provide useful probes of new physics at hadron colliders [1, 2]. Such signatures arise naturally in a broad class of models, including supersymmetry [3], large extra spatial dimensions [4], scenarios with weakly interacting massive particles [5], axion-like particles [6], and others. The ATLAS and CMS collaborations have performed searches for these topologies, placing constraints on many classes of new-physics models.

The possibility that quarks and leptons might not be elementary particles but instead composite objects built from more fundamental constituents (preons) has been discussed in the literature [7–9]. In compositeness models, excited fermions (f^*) emerge as phenomenological predictions of the underlying substructure [10]. Searches for f^* have been conducted at electron–positron, electron–proton, and hadron colliders over several decades. At LEP, these searches were performed in electron–positron collisions at centre-of-mass (\sqrt{s}) energies up to 209 GeV [11–15]. The HERA experiments searched for f^* in electron–proton collisions at \sqrt{s} up to 319 GeV [16–18]. CDF and D0 experiments at the Tevatron conducted searches for excited quarks (q^*) and excited charged leptons (ℓ^*) in proton–antiproton collisions at $\sqrt{s} = 1.8$ TeV and $\sqrt{s} = 1.96$ TeV [19]. At the LHC, both ATLAS and CMS have searched for q^* [20–30] and ℓ^* [31–40] in proton–proton (pp) collisions at $\sqrt{s} = 7, 8,$ and 13 TeV. Prospects for excited neutrino (ν^*), and ℓ^* searches at future lepton–hadron colliders have also been explored [41, 42]. However, dedicated searches for ν^* have been scarce. The most recent limits on ν^* were set by the ATLAS Collaboration in 2012 using 8 TeV pp collision data, excluding masses below 1.6 TeV [43]. No comparable constraints have been reported using the significantly larger Run 2 datasets collected at $\sqrt{s} = 13$ TeV,

leaving the high-mass regime unexplored. This motivates the reinterpretation of existing searches to assess their sensitivity to ν^* production.

In this work, we reinterpret selected ATLAS and CMS monojet and mono- V searches by using the published event selections, event yields and background expectations, and simulating the ν^* production. We derive 95% confidence-level (CL) upper limits on the production cross-section of ν^* as a function of their mass for benchmark assumptions governing the compositeness parameters. Although the systematic uncertainty treatment and ν^* signal simulation are less rigorous than in typical searches by the experimental collaborations, our results demonstrate the potential of ATLAS and CMS mono-object searches to largely extend the excluded part of the ν^* parameter space.

This paper is structured as follows. Section 2 introduces the theoretical framework describing ν^* , including their production and decay mechanisms. Section 3 details the simulation of signal events and detector response. Sections 4, and 5 describe the reinterpretation of the ATLAS monojet, and CMS monojet and mono- V searches. Conclusions are summarized in Section 6.

2 Theoretical Framework

The phenomenology of f^* is commonly described using the effective model introduced by Baur, Spira, and Zerwas (BSZ) [10]. The model assumes that f^* have the same spin as their SM counterparts but possess higher masses, which are not generated by the Higgs mechanism. In the BSZ approach, both left- and right-handed f^* components form $SU(2)$ doublets. The f^* doublets are represented as

$$F_{L/R}^* = \left(\begin{array}{c} (\nu_e^*)_{L/R} \\ e_{L/R}^* \end{array} \right), \left(\begin{array}{c} u_{L/R}^* \\ d_{L/R}^* \end{array} \right), \dots,$$

where ν_e^*, e^*, u^*, d^* stand for the excited electron neutrino, electron, up quark, and down quark, respectively, the subscripts L, R denote the chirality, and the ellipsis indicates the doublets of the second and third f^* generations.

Transitions between excited and ordinary fermions are enabled by two classes of effective operators in the BSZ model. The first consists of four-fermion contact interactions (CI), which correspond to a low-energy limit of new interactions among the preons:

$$\mathcal{L}_{\text{CI}} = \frac{2\pi}{\Lambda^2} j_\mu j^\mu, \quad (2.1)$$

where Λ is the compositeness scale and

$$j_\mu = \bar{F}_L \gamma_\mu F_L + \bar{F}_L^* \gamma_\mu F_L^* + \bar{F}_L^* \gamma_\mu F_L + \text{h.c.} \quad (2.2)$$

In the fermionic current j_μ , F_L stands for an SM doublet of fermions with respect to the $SU(2)$ group. At the LHC, ν^* are produced via the CI. Two example Feynman diagrams are shown in Fig. 1. The second class of operators consists of gauge-mediated interactions (GI). The corresponding Lagrangian, relevant for the ν^* decays, is given by

$$\mathcal{L}_{\text{GI}} = \frac{1}{2\Lambda} \bar{F}_R^* \sigma^{\mu\nu} \left(gf \frac{\tau^a}{2} W_{\mu\nu}^a + g' f' \frac{Y}{2} B_{\mu\nu} \right) F_L + \text{h.c.}, \quad (2.3)$$



Figure 1: Feynman diagrams for ν^* production via CI.

where f and f' are parameters reflecting the composite dynamics.

The ν^* particles decay through both CI and GI channels. CI-mediated decays, $\nu^* \rightarrow \nu q \bar{q}$, result in jets and $\mathbf{p}_T^{\text{miss}}$ in the final state. The GI decay modes are

$$\nu^* \rightarrow \nu \gamma, \quad \nu^* \rightarrow \nu Z, \quad \nu^* \rightarrow \ell W. \quad (2.4)$$

When the W or Z boson decays hadronically, the corresponding channel yields one or more jets in the final state. Commonly, $\mathbf{p}_T^{\text{miss}}$ arises from a neutrino that is either produced in the process depicted in Fig. 1a or from the GI decay to νZ . Given these production and decay mechanisms, an important part of ν^* events results in final states, which are targeted in ATLAS and CMS monojet and mono- V searches.

3 Signal Generation and Detector Simulation

Monte Carlo (MC) simulation is used to model the signal ν^* production processes considered in this analysis. All signal samples are generated for pp collisions at $\sqrt{s} = 13$ TeV, corresponding to the Run 2 operating conditions of the LHC. The production and decay of ν^* are simulated using PYTHIA 8.310 [44], employing the BSZ model to describe both CI production mechanisms and CI and GI decays. Only the single production of ν^* is considered, as the ν^* pair production cross-section is much smaller than the single production one [10]. Signal samples are generated for a discrete set of ν^* masses covering the range of $m_{\nu^*} = 600$ GeV–5000 GeV. The simulated mass points are chosen such that interpolation of the exclusion limits is possible. They are separated by 100 GeV in the regions 600–3000 GeV and 4400–5000 GeV, and by 50 GeV in the region 3000–4400 GeV. For each mass point, signal samples are generated for several choices of the f, f' parameters. Values $f = f' \in \{0.0, 0.2, 0.4, 0.6, 0.8, 1.0\}$ are used. Two benchmark settings of the compositeness scale are considered, $\Lambda = m_{\nu^*}$ and $\Lambda = 10$ TeV.

Detector effects are modelled using DELPHES 3.5.0 [45]. Two separate detector configurations are employed to approximate the response of the ATLAS and CMS detectors. They are encoded in detector cards, which are part of the DELPHES installation. In both configurations, jets are reconstructed using the anti- k_t algorithm [46] with a radius parameter of $R = 0.4$ (AK4). The threshold for the AK4 jet reconstruction is set to $p_T = 20$ GeV. A second jet collection is added to the CMS-like configuration, where jets are reconstructed

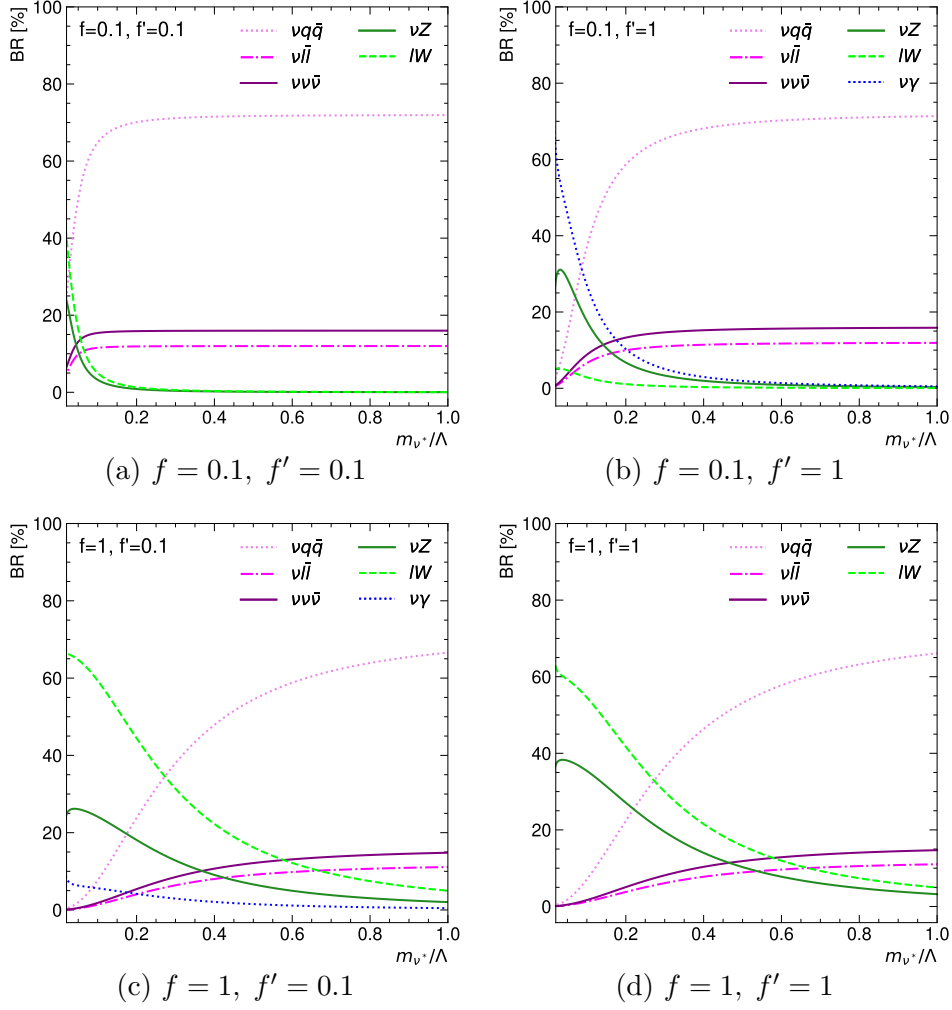


Figure 2: BRs of ν^* decays as a function of m_{ν^*}/Λ for $\Lambda = 10$ TeV and four configurations of the f, f' values.

using a larger radius parameter of $R = 0.8$ (AK8). It emulates the CMS reconstruction of boosted hadronic final states [2]. All simulated events are stored in ROOT [47] format and processed using a custom analysis framework implementing the event selections of the corresponding experimental analyses.

The ν^* branching ratios (BRs) are evaluated to learn in which phase space regions one can expect the signal. The BRs are calculated with PYTHIA and shown in Figure 2 as a function of m_{ν^*}/Λ for $\Lambda = 10$ TeV and four configurations of the f, f' values: $(f, f') = (0.1, 0.1), (0.1, 1), (1, 0.1),$ and $(1, 1)$. The CI decays, $\nu^* \rightarrow \nu q \bar{q}, \nu \ell \bar{\ell}, \nu \nu \bar{\nu}$, dominate for high values of m_{ν^*}/Λ or low values of the f, f' parameters. The $\nu q \bar{q}$ channel largely dominates the CI decays. The GI decays, $\nu^* \rightarrow \nu Z$, and ℓW , become significant for low values of m_{ν^*}/Λ and high values of the f, f' parameters. The BR of the ℓW channel increases with f . The νZ and $\nu \gamma$ channels are the dominant GI decays when f' is large, and f is small. The $\nu \gamma$ decay is forbidden when $f = f'$.

4 Reinterpretation of the ATLAS monojet search

The ATLAS search presented in Ref. [1] is based on events with a high- p_T jet and large magnitude of the missing transverse momentum, E_T^{miss} . It uses the full 13 TeV pp Run 2 dataset collected by the ATLAS detector [48] corresponding to an integrated luminosity of 139 fb^{-1} . Events are required to contain at least one AK4 jet with $p_T > 150 \text{ GeV}$ and $|\eta| < 2.4$, and no more than three additional AK4 jets with $p_T > 30 \text{ GeV}$ and $|\eta| < 2.8$. In the signal region (SR), E_T^{miss} is required to be larger than 200 GeV . Additional SR selection criteria, like veto of electrons, muons, photons, or presence of hadronically decaying tau leptons in the event, quality requirements on the leading- p_T jet reconstruction, and angular separation between $\mathbf{p}_T^{\text{miss}}$ and each jet, are described in Ref. [1].

The dominant SM background arises from $Z(\nu\nu)$ +jets production, with additional contributions from $W(\ell\nu)$ +jets, top-quark, and diboson processes. Dedicated control regions (CRs) enriched in $Z(\ell\ell)$ +jets, $W(\ell\nu)$ +jets, and $t\bar{t}$ events are used to improve the background prediction, which is mostly based on MC simulation. Each region is binned in the magnitude of the $\mathbf{p}_T^{\text{recoil}}$ vector, p_T^{recoil} ; $\mathbf{p}_T^{\text{recoil}}$ is a proxy for the transverse momentum of the system which recoils against the hadronic activity in the event. In the SR, p_T^{recoil} is equal to E_T^{miss} . The ATLAS analysis provides an SR background estimate determined in a simultaneous background-only profile likelihood fit to the CRs together with its total uncertainty and the total data yield in each bin [49].

The present study uses the profile likelihood ratio hypothesis test [50] and the CL_s method [51, 52] to derive exclusion limits on the ν^* model parameters. The study uses the asymptotic distributions [50] of the test statistic under the signal-plus-background and background-only hypotheses to evaluate the corresponding p -values needed in the CL_s method. All SR bins defined in Ref. [1] are used in the test. The background estimate provided by the ATLAS analysis is used as the background template in the likelihood construction. For each setting of the Λ , m_{ν^*} , f , f' values, the signal template is obtained by applying the SR selection to the corresponding simulated signal sample. The event yield in each bin is treated as a Poisson-distributed variable, and the likelihood includes the product of the Poisson probabilities across all SR bins. The expectation value of each Poisson term is the sum of the signal and background contributions in the corresponding bin. The signal contribution is scaled by a signal strength parameter, which is the parameter of interest in the test. The likelihood also includes the total background uncertainty in the form of one Gaussian-constrained nuisance parameter. The total uncertainty is treated as correlated across all SR bins. The likelihood functions are built, and all statistical tests are performed using the HISTFITTER package [53].

A key aspect of the reinterpretation is ensuring its logical consistency. Since the ATLAS analysis relies on CRs to normalize and shape the background prediction, a significant signal contamination in these regions could invalidate the post-fit background estimate. If the signal existed and was present in the CRs, it would bias the background prediction in the CRs and the SR. To address this, the ν^* signal yields are computed for all ATLAS CRs: $W(\mu\nu)$, $W(e\nu)$, $Z(\mu\mu)$, $Z(ee)$, and $t\bar{t}$. As the signal is expected to be most prominent in the high- p_T^{recoil} part of each CR, the signal and background yields are compared there.

In each CR, a subregion is defined with a requirement on $p_{\text{T}}^{\text{recoil}}$ to be above a certain threshold, $p_{\text{T}}^{\text{recoil, th}}$. The threshold is chosen such that the signal yield in that subregion is non-zero, with a statistical significance of at least 2σ , for $m_{\nu^*} = 1400$ GeV, $\Lambda = m_{\nu^*}$, and any value of $f = f'$. The value $p_{\text{T}}^{\text{recoil, th}} = 600$ GeV satisfies this requirement for all CRs and ν^* flavours. If the signal yield exceeds 10% of the background in the high- $p_{\text{T}}^{\text{recoil}}$ subregion of any CR, the corresponding point in the ν^* model parameter space is deemed unreliable for reinterpretation. When the Λ parameter is set to 10 TeV, and $f = f'$, the signal contamination is negligible in all CRs for all values of m_{ν^*} between 600 GeV and 4000 GeV (steps of 400 GeV are made), all values of f between 0 and 1 (steps of 0.2 are made), and all ν^* flavours. The excited tau neutrino (ν_{τ}^*) signal contamination exceeds the 10% threshold when $\Lambda = m_{\nu_{\tau}^*}$, and $m_{\nu_{\tau}^*} \leq 1.4$ TeV. With this setting, the $t\bar{t}$ CR turns out to have the highest relative ν_{τ}^* signal contamination. Figure 3a displays the ν_{τ}^* signal-to-background ratio (S/B) in its high- $p_{\text{T}}^{\text{recoil}}$ subregion. Masses $m_{\nu_{\tau}^*} \leq 1.4$ TeV are excluded from the subsequent statistical test of the $\Lambda = m_{\nu_{\tau}^*}$ scenario for all values of $f = f'$. The same constraints are obtained for the ν_e^* signal. For the excited muon neutrino (ν_{μ}^*) signal, the signal contamination is the most prominent in the $W(\mu\nu)$ CR. Parameter space points with $m_{\nu_{\mu}^*} \leq 1$ TeV ($m_{\nu_{\mu}^*} \leq 1.4$ TeV) are excluded from the statistical test of the $\Lambda = m_{\nu_{\mu}^*}$ scenario for all values of $f = f'$ (for $f = f' \geq 0.4$).

Figure 3b presents 95% CL upper limits on the ν_{τ}^* production cross-section as a function of $m_{\nu_{\tau}^*}$. The model parameters are set in the following way: $\Lambda = m_{\nu_{\tau}^*}$, $f = f' = 1$. The observed cross-section limit is 6 – 8 fb for all $m_{\nu_{\tau}^*}$ values between 2 TeV and 4.5 TeV, and it is within the 2σ band around the expected limit. The observed mass lower limit is ~ 3900 GeV. Figure 4a presents 95% CL exclusion contours in the $(m_{\nu_{\tau}^*}, f)$ plane for the $\Lambda = m_{\nu_{\tau}^*}$ scenario. The observed limit is ~ 3900 GeV for all f values, and it is within the 2σ band around the expected limit. The limits on ν_e^* and ν_{μ}^* are evaluated in analogy with the ν_{τ}^* limits. They are shown in Figure 4b together with the ν_{τ}^* contour. The observed mass lower limits are ~ 3900 GeV for all ν^* flavours, and values of $f = f'$. The lack of f dependence is expected, as the f -sensitive GI decays are suppressed when $\Lambda = m_{\nu^*}$.

5 Reinterpretation of the CMS monojet and mono- V search

The CMS search presented in Ref. [2] is based on events with a high- p_{T} jet and large magnitude of $\mathbf{p}_{\text{T}}^{\text{miss}}$, denoted as $p_{\text{T}}^{\text{miss}}$ in the CMS paper and this section. It uses 13 TeV pp collision data collected by the CMS detector [54] in 2017 and 2018, corresponding to an integrated luminosity of 101 fb^{-1} . It employs machine learning techniques to define two complementary final-state categories: a monojet category targeting events with narrow jets from initial-state radiation, and a mono- V category optimised for events with large-radius jets consistent with hadronic decays of W or Z bosons. In the SR, $p_{\text{T}}^{\text{miss}}$ is required to be larger than 250 GeV. The mono- V category requires the leading- p_{T} AK8 jet to have $p_{\text{T}} > 250$ GeV, $|\eta| < 2.4$, be V tagged with the DEEPAK8 algorithm [55], and have a mass, modified with the soft-drop algorithm [56, 57], compatible with that of a W or Z boson. The mono- V category is further divided into two SRs, low- and high-purity mono- V , depending on the DEEPAK8 score. Events not satisfying the mono- V criteria are

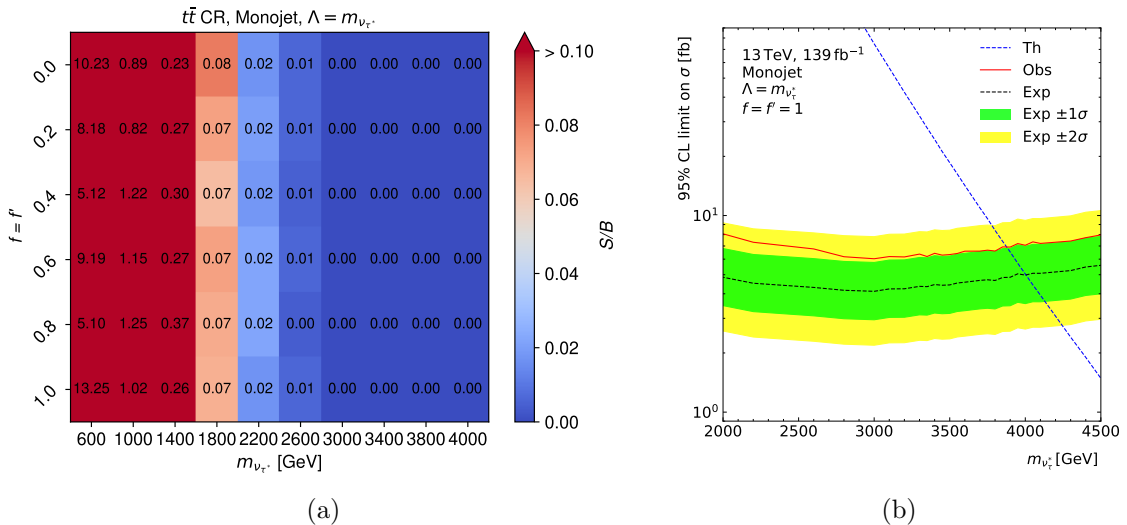


Figure 3: (a) The S/B of ν_τ^* events in the high- p_T^{recoil} subregion of the ATLAS $t\bar{t}$ CR as a function of $m_{\nu_\tau^*}$ and f . The p_T^{recoil} threshold is 600 GeV. The Λ parameter is set equal to $m_{\nu_\tau^*}$, and $f' = f$. The dark red colour highlights $(m_{\nu_\tau^*}, f)$ points with signal yield higher than 10% of the post-fit background estimate. (b) The 95% CL upper limit on the ν_τ^* production cross-section as a function of $m_{\nu_\tau^*}$ for $\Lambda = m_{\nu_\tau^*}$, and $f = f' = 1$. The observed (expected) limit is shown in a solid red (dashed black) line. Boundaries of the green (yellow) band display $\pm 1\sigma$ ($\pm 2\sigma$) uncertainty in the expected limit. The dashed blue line displays the theoretical cross-section. The limits are based on the ATLAS monojet search results.

assigned to the monojet category if the leading- p_T AK4 jet has $p_T > 100$ GeV, $|\eta| < 2.4$, and passes additional good quality criteria. Additional SR selection criteria, such as the veto of electrons, muons, photons, hadronically decaying tau leptons, or the presence of b -tagged jets in the event, angular separation between $\mathbf{p}_T^{\text{miss}}$ and jets, or similarity between the default and calorimeter-based p_T^{miss} value, are described in Ref. [2].

The present reinterpretation study emulates the DEEPAK8 algorithm decision by applying the efficiency rates quoted in Ref. [2] to the leading- p_T AK8 jet in each event. The fraction of events contributing to the high-purity mono- V sample is 30% (40%) when the jet is truth-matched to a hadronically decaying W or Z boson and has $p_T = 250$ GeV ($p_T > 800$ GeV). A linear interpolation is used to determine the fraction of events in the $p_T \in (250, 800)$ GeV region. When the leading- p_T AK8 jet is not truth-matched to a hadronically decaying W or Z boson, the fraction of events contributing to the high-purity mono- V sample is 0.7%. From events which are not added to the high-purity mono- V sample, a fraction of 40% (7%), resp. 30% (5%) is assigned to the low-purity mono- V sample when the leading- p_T AK8 jet is (is not) truth-matched to a hadronically decaying W or Z boson and has $p_T = 250$ GeV, resp. $p_T > 800$ GeV. A linear interpolation of the efficiency rates is used in the $p_T \in (250, 800)$ GeV region.

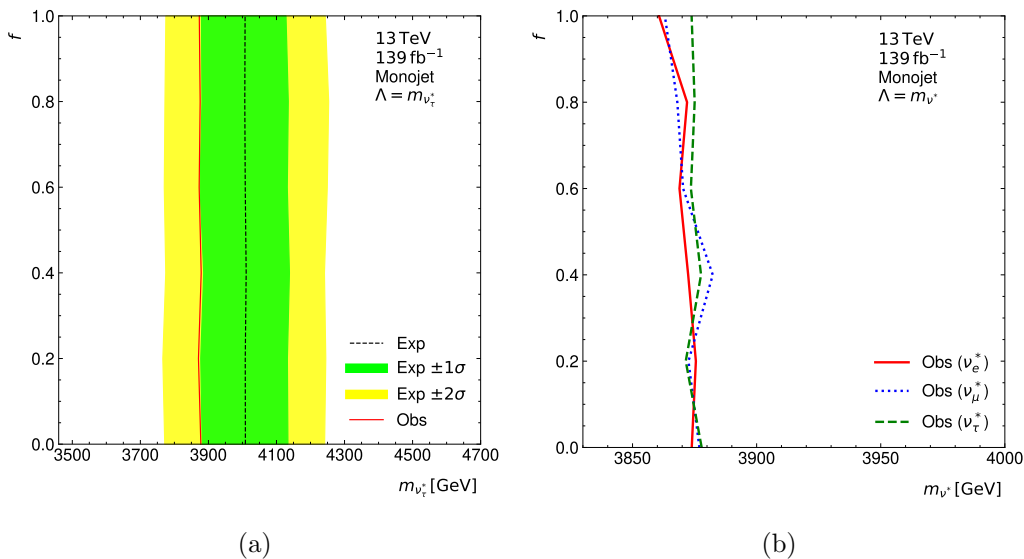


Figure 4: Limits based on the ATLAS monojet search results. (a) 95% CL exclusion contours in the $(m_{\nu_\tau^*}, f)$ plane for the $\Lambda = m_{\nu_\tau^*}$, $f = f'$ scenario. The observed (expected) limit is shown in a solid red (dashed black) line. Boundaries of the green (yellow) band display $\pm 1\sigma$ ($\pm 2\sigma$) uncertainty in the expected limit. (b) Observed 95% CL exclusion contours for all three ν^* flavours in the (m_{ν^*}, f) plane for the $\Lambda = m_{\nu^*}$, $f = f'$ scenario. The solid red, dotted blue, and dashed green lines display the observed limits on the ν_e^* , ν_μ^* , and ν_τ^* models, respectively.

The dominant SM backgrounds arise from $Z(\nu\nu)+\text{jets}$, $W(\ell\nu)+\text{jets}$, and $\gamma+\text{jets}$ production, with smaller contributions from $t\bar{t}$, diboson, and multijet processes. The SRs, low-purity mono- V , high-purity mono- V , and monojet, are binned in $p_{\text{T}}^{\text{miss}}$. The background in the SRs is estimated using MC simulation together with data from CRs enriched in $W(\mu\nu)$, $W(e\nu)$, $Z(\mu\mu)$, $Z(ee)$, and $\gamma+\text{jets}$ events. The CRs are binned in the magnitude of the hadronic recoil transverse momentum, which is a quantity analogous to the $p_{\text{T}}^{\text{recoil}}$ variable defined in the ATLAS monojet analysis. It will be denoted as $p_{\text{T}}^{\text{recoil}}$ hereafter. The CMS analysis provides a SR background estimate determined in a simultaneous background-only profile likelihood fit to the CRs, and it provides the data yield in each SR bin [58]. It also provides the covariance matrix of nuisance parameters associated with the background estimate in the simplified likelihood approach [59]. The signal template is obtained by applying the SR selection to the corresponding simulated signal sample for each setting of the Λ , m_{ν^*} , f , f' values. The present study uses these inputs to construct the simplified likelihood function. Apart from the likelihood construction, the limit setting strategy is the same as described in Section 4. A custom script based on the `iminuit` package [60, 61] is used to build the simplified likelihood function and perform the statistical tests.

The present study does the same check for potential signal contamination in the CMS CRs to ensure the reinterpretation's logical consistency, as described in Section 4. For

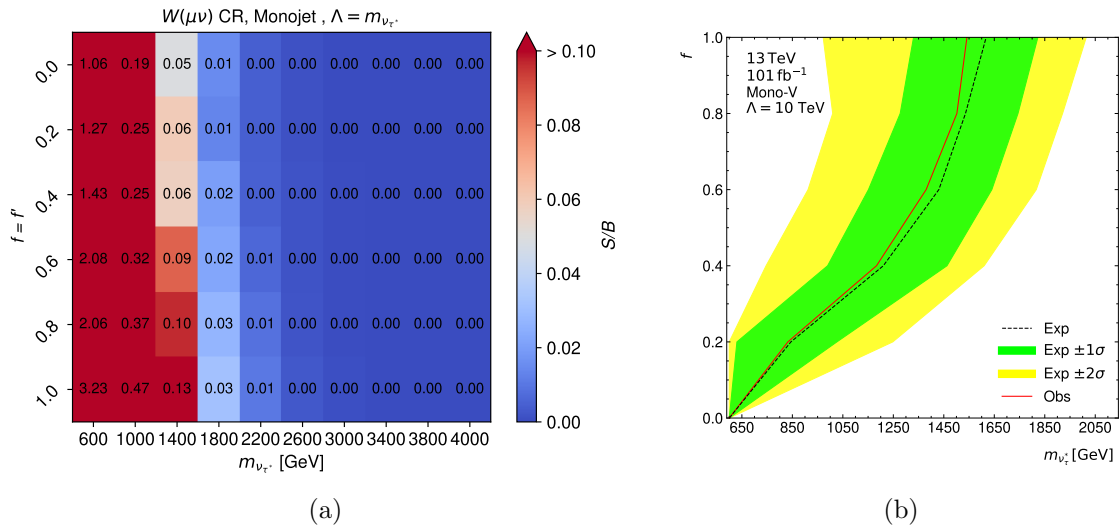


Figure 5: (a) S/B of ν_τ^* events in the high- p_T^{recoil} subregion of the CMS $W(\mu\nu)$ CR as a function of $m_{\nu_\tau^*}$ and f . The p_T^{recoil} threshold is 600 GeV. The Λ parameter is set equal to $m_{\nu_\tau^*}$, and $f' = f$. The dark red colour highlights $(m_{\nu_\tau^*}, f)$ points with signal yield higher than 10% of the post-fit background estimate. (b) 95% CL exclusion contours in the $(m_{\nu_\tau^*}, f)$ plane for the $\Lambda = 10$ TeV, $f = f'$ scenario. The observed (expected) limit is shown in a solid red (dashed black) line. Boundaries of the green (yellow) band display $\pm 1\sigma$ ($\pm 2\sigma$) uncertainty in the expected limit. The limits are based on the CMS mono- V search results.

all monojet and mono- V categories, all CRs, and all ν^* flavours, the 600 GeV threshold on p_T^{recoil} is found to satisfy the requirement described in Section 4, and is used to define the high- p_T^{recoil} subregion of each CR. When the Λ parameter is set to 10 TeV, the signal contamination is negligible in the high- p_T^{recoil} subregion of each CR for all the monojet and mono- V categories and all the considered ν^* scenarios. The situation is different when $\Lambda = m_{\nu^*}$. In the monojet category, the single muon, $W(\mu\nu)$, CR is the most affected by the ν_τ^* and ν_μ^* signal contamination, excluding the following parameter space points from the statistical test: $m_{\nu_\tau^*}, m_{\nu_\mu^*} \leq 1$ TeV for all $f = f'$ values, and $m_{\nu_\tau^*} (m_{\nu_\mu^*}) \leq 1.4$ TeV for $f = f' \geq 0.8$ (0.6). Similarly, the $W(e\nu)$ CR is the most affected by the ν_e^* signal contamination, excluding $m_{\nu_e^*} \leq 1$ TeV for all $f = f'$ values, and $m_{\nu_e^*} \leq 1.4$ TeV for $f = f' \geq 0.6$. Figure 5a displays S/B for the ν_τ^* signal in the high- p_T^{recoil} subregion of the $W(\mu\nu)$ monojet CR. Regarding the mono- V categories, a point in the ν^* model parameter space is excluded from the statistical test if the S/B is above the 10% threshold in a certain high- p_T^{recoil} CR subregion in either the low-purity or high-purity mono- V category. For high $f = f'$ values, masses up to 2.2 TeV are not used in the statistical test.

The present study uses the monojet and mono- V categories separately in the statistical analysis to show their individual sensitivities to the ν^* model. When $\Lambda = 10$ TeV, the monojet category cannot be used to set limits on the ν^* model for the considered mass range $m_{\nu^*} \geq 600$ GeV, as it shows too little sensitivity to this type of signal. The mono- V

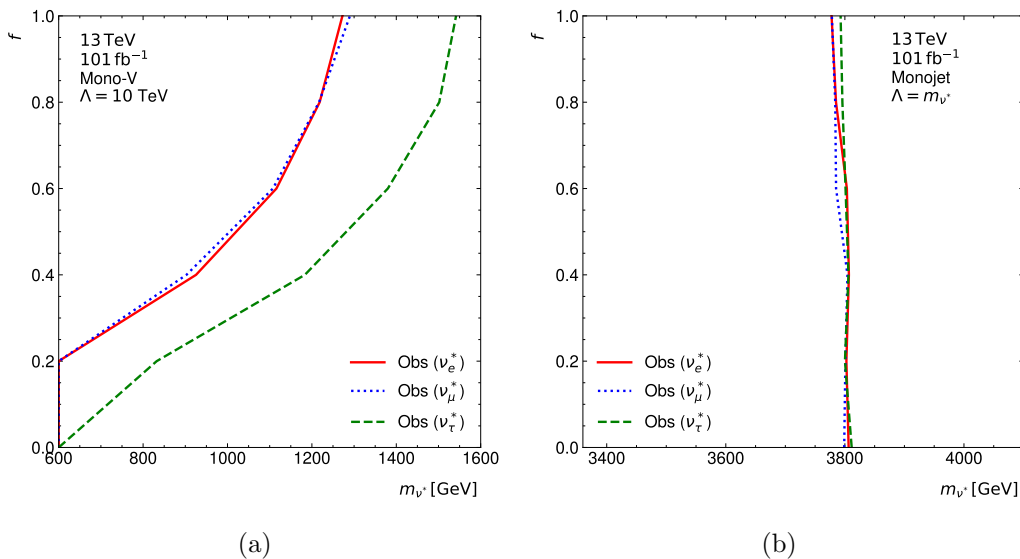


Figure 6: (a) Observed 95% CL exclusion contours for all three ν^* flavours in the (m_{ν^*}, f) plane for the $\Lambda = 10$ TeV, $f = f'$ scenario based on the CMS mono- V search results. (b) Observed 95% CL exclusion contours for all three ν^* flavours in the (m_{ν^*}, f) plane for the $\Lambda = m_{\nu^*}$, $f = f'$ scenario based on the CMS monojet search results. The solid red, dotted blue, and dashed green lines display the observed limits on the ν_e^* , ν_μ^* , and ν_τ^* models, respectively.

SRs turn out to be sensitive to this part of the parameter space, particularly for high values of $f = f'$. The low- and high-purity mono- V SRs are used simultaneously in the statistical test to set limits on the ν^* model. Figure 5b shows the 95% CL exclusion contours in the $(m_{\nu_\tau^*}, f)$ plane for the $f = f'$ scenario. The $m_{\nu_\tau^*}$ limit reaches ~ 1.5 TeV for $f = f' = 1$. It is within the 1σ band around the expected limit. Figure 6a shows the observed mono- V -data-based exclusion contours in the (m_{ν^*}, f) parameter plane for all three ν^* flavours, $\Lambda = 10$ TeV, and $f = f'$. The limits on $m_{\nu_e^*}$ and $m_{\nu_\mu^*}$ are less stringent than the $m_{\nu_\tau^*}$ ones. In the considered parameter space region, the dominant decay channel is $\nu^*(Wl)$. The SRs accept more of these events for the ν_τ^* signal than for the ν_e^* and ν_μ^* signals, as it is more likely to misreconstruct a hadronically decaying τ lepton as a jet than the e or μ leptons. When $\Lambda = m_{\nu^*}$, the monojet category is more sensitive to the ν^* signal than the mono- V one. Figure 6b shows the observed monojet-data-based exclusion contours in the (m_{ν^*}, f) parameter plane for all three ν^* flavours, $\Lambda = m_{\nu^*}$, and $f = f'$. The observed mass limits are ~ 3800 GeV with almost no dependence on f . These limits are compatible with the corresponding limits based on the ATLAS monojet search results.

6 Conclusion

This work presents a reinterpretation of ATLAS and CMS monojet and mono- V searches based on the LHC Run 2 pp data in the context of the BSZ ν^* model. The most recent limit on ν^* mass was set by ATLAS in 2012, using the 8 TeV pp LHC Run 1 data, excluding

masses below 1.6 TeV. No comparable constraints have been reported using the significantly larger Run 2 datasets. The present study demonstrates the potential of the ATLAS and CMS Run 2 monojet searches to exclude ν^* with masses up to almost 4 TeV for all three ν^* flavours at 95% CL when $\Lambda = m_{\nu^*}$. This limit shows no significant dependence on the coupling parameters f and f' , as the monojet SRs are mostly populated by ν^* CI decays when $\Lambda = m_{\nu^*}$. The CMS mono- V search has the potential to constrain a complementary region of the parameter space, with lower ν^* masses, high Λ and high f, f' . The mass limit can reach up to ~ 1.5 TeV for $f = f' = 1$ and $\Lambda = 10$ TeV.

This paper is accompanied by a GitLab repository [62] providing cross-section limits for all ν^* flavours, $f = f'$ values and both benchmark Λ settings. It also provides expected limits in the (m_{ν^*}, f) plane for all three ν^* flavours and both Λ settings, as well as more details on the high- p_T^{recoil} CR subregion signal contamination studies.

Acknowledgments

This work was supported by the Grant Agency of Charles University (GA UK), project No. 284222.

Data Availability Statement

This article has no associated data or the data will not be deposited.

Code Availability Statement

This article has no associated code or the code will not be deposited.

References

- [1] ATLAS Collaboration, *Search for new phenomena in events with an energetic jet and missing transverse momentum in pp collisions at $\sqrt{s} = 13$ TeV with the ATLAS detector*, *Phys. Rev. D* **103** (2021) 112006 [[2102.10874](#)].
- [2] CMS Collaboration, *Search for new particles in events with energetic jets and large missing transverse momentum in proton–proton collisions at $\sqrt{s} = 13$ TeV*, *JHEP* **11** (2021) 153 [[2107.13021](#)].
- [3] Y.A. Golfand and E.P. Likhtman, *Extension of the Algebra of Poincare Group Generators and Violation of p Invariance*, *JETP Lett.* **13** (1971) 323.
- [4] N. Arkani-Hamed, S. Dimopoulos and G.R. Dvali, *The Hierarchy problem and new dimensions at a millimeter*, *Phys. Lett. B* **429** (1998) 263 [[hep-ph/9803315](#)].
- [5] G. Steigman and M.S. Turner, *Cosmological Constraints on the Properties of Weakly Interacting Massive Particles*, *Nucl. Phys. B* **253** (1985) 375.
- [6] Mimasu, Ken and Sanz, Verónica, *ALPs at colliders*, *JHEP* **06** (2015) 173 [[1409.4792](#)].
- [7] H. Terazawa, *Subquark model of leptons and quarks*, *Phys. Rev. D* **22** (1980) 184.
- [8] H. Harari, *A schematic model of quarks and leptons*, *Phys. Lett. B* **86** (1979) 83.

- [9] H. Fritzsch and G. Mandelbaum, *Weak interactions as manifestations of the substructure of leptons and quarks*, *Phys. Lett. B* **102** (1981) 319.
- [10] U. Baur, M. Spira and P.M. Zerwas, *Excited-quark and -lepton production at hadron colliders*, *Phys. Rev. D* **42** (1990) 815.
- [11] L3 Collaboration, *Search for excited leptons at LEP*, *Phys. Lett. B* **568** (2003) 23 [[hep-ex/0306016](#)].
- [12] OPAL Collaboration, *Search for charged excited leptons in $e+e-$ collisions at $\sqrt{s} = 183 - 209$ GeV*, *Phys. Lett. B* **544** (2002) 57.
- [13] DELPHI Collaboration, *Search for excited leptons in $e+e-$ collisions at $\sqrt{s} = 189 - 209$ GeV*, *Eur. Phys. J. C* **46** (2006) 277 [[hep-ex/0603045](#)].
- [14] DELPHI Collaboration, *Search for composite and exotic fermions at LEP 2*, *Eur. Phys. J. C* **8** (1999) 41 [[hep-ex/9811005](#)].
- [15] ALEPH Collaboration, *Search for evidence of compositeness at LEP I*, *Eur. Phys. J. C* **4** (1998) 571.
- [16] S. Chekanov, M. Derrick, D. Krakauer, S. Magill, B. Musgrave, A. Pellegrino et al., *Searches for excited fermions in ep collisions at HERA*, *Phys. Lett. B* **549** (2002) 32.
- [17] F. Aaron, C. Alexa, V. Andreev, B. Antunovic, S. Aplin, A. Asmone et al., *A search for excited neutrinos in e^-p collisions at HERA*, *Phys. Lett. B* **663** (2008) 382.
- [18] F. Aaron, C. Alexa, K. Alimujiang, V. Andreev, B. Antunovic, A. Asmone et al., *Search for excited quarks in ep collisions at HERA*, *Phys. Lett. B* **678** (2009) 335.
- [19] D. Toback and L. Živković, *Review of Physics Results from the Tevatron: Searches for New Particles and Interactions*, *Int. J. Mod. Phys. A* **30** (2015) 1541007 [[1409.4910](#)].
- [20] ATLAS Collaboration, *Search for the production of single vector-like and excited quarks in the Wt final state in pp collisions at $\sqrt{s} = 8$ TeV with the ATLAS detector*, *JHEP* **02** (2016) 110 [[1510.02664](#)].
- [21] ATLAS Collaboration, *Search for new phenomena in dijet events using 37 fb^{-1} of pp collision data collected at $\sqrt{s} = 13$ TeV with the ATLAS detector*, *Phys. Rev. D* **96** (2017) 052004 [[1703.09127](#)].
- [22] ATLAS Collaboration, *Search for resonances in the mass distribution of jet pairs with one or two jets identified as b -jets in proton-proton collisions at $\sqrt{s} = 13$ TeV with the ATLAS detector*, *Phys. Rev. D* **98** (2018) 032016 [[1805.09299](#)].
- [23] ATLAS Collaboration, *Search for new phenomena in the dijet mass distribution using pp collision data at $\sqrt{s} = 8$ TeV with the ATLAS detector*, *Phys. Rev. D* **91** (2015) 052007 [[1407.1376](#)].
- [24] ATLAS Collaboration, *Search for single b^* -quark production with the ATLAS detector at $\sqrt{s} = 7$ TeV*, *Phys. Lett. B* **721** (2013) 171 [[1301.1583](#)].
- [25] ATLAS Collaboration, *Search for new phenomena in dijet mass and angular distributions from pp collisions at $\sqrt{s} = 13$ TeV with the ATLAS detector*, *Phys. Lett. B* **754** (2016) 302 [[1512.01530](#)].
- [26] CMS Collaboration, *Search for pair production of excited top quarks in the lepton+jets final state*, *JHEP* **06** (2014) 125 [[1311.5357](#)].

- [27] CMS Collaboration, *Search for excited quarks in the γ +jet final state in proton–proton collisions at $\sqrt{s} = 8$ TeV*, *Phys. Lett. B* **738** (2014) 274 [[1406.5171](#)].
- [28] CMS Collaboration, *Search for the production of an excited bottom quark decaying to tW in proton–proton collisions at $\sqrt{s} = 8$ TeV*, *JHEP* **01** (2016) 166 [[1509.08141](#)].
- [29] CMS Collaboration, *Search for excited quarks of light and heavy flavor in γ +jet final states in proton–proton collisions at $\sqrt{s} = 13$ TeV*, *Phys. Lett. B* **781** (2018) 390 [[1711.04652](#)].
- [30] CMS Collaboration, *Search for dijet resonances with data scouting in proton–proton collisions at $\sqrt{s} = 13$ TeV*, [2510.21641](#).
- [31] ATLAS Collaboration, *Search for excited leptons in proton–proton collisions at $\sqrt{s} = 7$ TeV with the ATLAS detector*, *Phys. Rev. D* **85** (2012) 072003 [[1201.3293](#)].
- [32] ATLAS Collaboration, *Search for excited electrons and muons in $\sqrt{s} = 8$ TeV proton–proton collisions with the ATLAS detector*, *New J. Phys.* **15** (2013) 093011 [[1308.1364](#)].
- [33] ATLAS Collaboration, *A search for an excited muon decaying to a muon and two jets in pp collisions at $\sqrt{s} = 8$ TeV with the ATLAS detector*, *New J. Phys.* **18** (2016) 073021 [[1601.05627](#)].
- [34] ATLAS Collaboration, *Search for excited electrons singly produced in proton–proton collisions at $\sqrt{s} = 13$ TeV with the ATLAS experiment at the LHC*, *Eur. Phys. J. C* **79** (2019) 803 [[1906.03204](#)].
- [35] ATLAS Collaboration, *Search for excited τ -leptons and leptoquarks in the final state with τ -leptons and jets in pp collisions at $\sqrt{s} = 13$ TeV with the ATLAS detector*, *JHEP* **06** (2023) 199 [[2303.09444](#)].
- [36] CMS Collaboration, *A search for excited leptons in pp collisions at $\sqrt{s} = 7$ TeV*, *Phys. Lett. B* **704** (2011) 143 [[1107.1773](#)].
- [37] CMS Collaboration, *Search for excited leptons in pp collisions at $\sqrt{s} = 7$ TeV*, *Phys. Lett. B* **720** (2013) 309 [[1210.2422](#)].
- [38] CMS Collaboration, *Search for excited leptons in proton–proton collisions at $\sqrt{s} = 8$ TeV*, *JHEP* **03** (2016) 125 [[1511.01407](#)].
- [39] CMS Collaboration, *Search for excited leptons in $\ell\ell\gamma$ final states in proton–proton collisions at $\sqrt{s} = 13$ TeV*, *JHEP* **04** (2019) 015 [[1811.03052](#)].
- [40] CMS Collaboration, *Search for excited tau leptons in the $\tau\tau\gamma$ final state in proton–proton collisions at $\sqrt{s} = 13$ TeV*, *JHEP* **06** (2024) 006 [[2410.21137](#)].
- [41] A. Caliskan, *Excited neutrino search potential of the fcc-based electron-hadron colliders*, *Adv. High Energy Phys.* **2017** (2017) 4726050 [[1706.09797](#)].
- [42] A. Caliskan and S.O. Kara, *Single production of the excited electrons in the future fcc-based lepton–hadron colliders*, *Int. J. Mod. Phys. A* **33** (2018) 1850141 [[1806.02037](#)].
- [43] ATLAS Collaboration, *Search for new phenomena in events with three or more charged leptons in pp collisions at $\sqrt{s} = 8$ TeV with the ATLAS detector*, *JHEP* **08** (2015) 138 [[1411.2921](#)].
- [44] C. Bierlich, S. Chakraborty, N. Desai, L. Gellersen, I. Helenius, P. Ilten et al., *A comprehensive guide to the physics and usage of PYTHIA 8.3*, *SciPost Phys. Codeb.* (2022) [[2203.11601](#)].

- [45] DELPHES 3 Collaboration, *DELPHES 3: a modular framework for fast simulation of a generic collider experiment*, *JHEP* **02** (2014) 057 [[1307.6346](#)].
- [46] M. Cacciari, G.P. Salam and G. Soyez, *The anti- k_t jet clustering algorithm*, *JHEP* **04** (2008) 063 [[0802.1189](#)].
- [47] R. Brun and F. Rademakers, *Root – an object oriented data analysis framework*, *Nucl. Instrum. Meth. A* **389** (1997) 81.
- [48] Garelli, Nicoletta, *Performance of the ATLAS Detector in Run-2*, *EPJ Web Conf.* **164** (2017) 01021.
- [49] ATLAS Collaboration, *Search for new phenomena in events with an energetic jet and missing transverse momentum in pp collisions at $\sqrt{s} = 13$ TeV with the ATLAS detector*, *HEPData (collection)* (2025) .
- [50] G. Cowan, K. Cranmer, E. Gross and O. Vitells, *Asymptotic formulae for likelihood-based tests of new physics*, *Eur. Phys. J. C* **71** (2011) 1554 [[1007.1727](#)].
- [51] T. Junk, *Confidence level computation for combining searches with small statistics*, *Nucl. Instrum. Meth. A* **434** (1999) 435 [[hep-ex/9902006](#)].
- [52] A.L. Read, *Presentation of search results: the CL_s technique*, *J. Phys. G* **28** (2002) 2693.
- [53] M. Baak, G. Besjes, D. Côté, A. Koutsman, J. Lorenz and D. Short, *HistFitter software framework for statistical data analysis*, *Eur. Phys. J. C* **75** (2015) 153 [[1410.1280](#)].
- [54] CMS collaboration, *Overview of the CMS Detector Performance at LHC Run 2*, *Universe* **5** (2019) 18.
- [55] CMS Collaboration, *Identification of heavy, energetic, hadronically decaying particles using machine-learning techniques*, *JINST* **15** (2020) P06005 [[2004.08262](#)].
- [56] M. Dasgupta, A. Fregoso, S. Marzani and G.P. Salam, *Towards an understanding of jet substructure*, *JHEP* **09** (2013) 029 [[1307.0007](#)].
- [57] J.M. Butterworth, A.R. Davison, M. Rubin and G.P. Salam, *Jet substructure as a new higgs-search channel at the large hadron collider*, *Phys. Rev. Lett.* **100** (2008) 242001 [[0802.2470](#)].
- [58] CMS Collaboration, *Search for new particles in events with energetic jets and large missing transverse momentum in proton-proton collisions at $\sqrt{s} = 13$ TeV*, *HEPData (collection)* (2022) .
- [59] CMS Collaboration, *Simplified likelihood for the re-interpretation of public CMS results*, *CERN-CMS-NOTE-2017-001* (2017) .
- [60] H. Dembinski, P. Ongmongkolkul et al., *scikit-hep/iminuit*, *Zenodo* (2020) .
- [61] F. James and M. Roos, *Minuit: A System for Function Minimization and Analysis of the Parameter Errors and Correlations*, *Comput. Phys. Commun.* **10** (1975) 343.
- [62] G. Karkosova Martinovicova and V. Pleskot, *Reinterpretation of ATLAS and CMS mono-jet and mono- V searches in terms of excited neutrinos: public figures*, *GitLab Repository*, https://gitlab.mff.cuni.cz/martinog/excnu_reinterpretation (2026) .